

Electron and Spin Density Topology of the H-Cluster and Its Biomimetic Complexes

Logan J. Giles,^[a] Alexios Grigoropoulos,^[a] and Robert K. Szilagyi*^[a]

Keywords: Cluster compounds / Electronic structure / Spin density / Electron density critical points / Density functional calculations / [FeFe]-hydrogenase

The catalytically active cluster of [FeFe]-hydrogenase (H-cluster) is unique due to its chemical composition and electronic and geometric structures. Protein crystallography revealed the presence of biologically unique diatomic ligands coordinating to the Fe centers and three light atoms bridging the sulfur atoms of its [2Fe]-subcluster. The identity of the light atoms remains uncertain, even at close to atomic resolution (1.39 Å), as well as due to the lack of understanding at the molecular level of the cluster's biosynthetic pathway. By using all of the proposed ligand compositions, we carried out a comprehensive electronic structure analysis by evaluating the topology of the electron density and, particularly, the atomic spin density distribution derived from various population analysis methods for the free dithiolate ligands, the biomimetic [2Fe] complexes, and the entire H-cluster embedded in its approximately 3.5 Å protein environment. In the biomimetic model complexes we found substantial spin density de-

localization at the bridgehead of the dithiolate ligands. We attributed the presence of spin density to the through-space spin polarization interaction between the paramagnetic iron centers and the bridgehead group, as represented by the ring critical points for the [Fe-(S-R-S)-Fe] metallacycles. However, this spin polarization of the bridgehead group vanishes for some of the biomimetic models, as well as for the 208-atom computational model of the H-cluster, due to a network of weak interactions. When the bridgehead group becomes part of a conduit for transmitting the spin polarization towards the terminal ends of each interaction network, such as the distal water or H-bonded residues, the spin density vanishes. The variations of the Fe atomic spin densities were compared and contrasted for the proximal and distal iron sites in the crystallographic and the rotated conformations, respectively.

Introduction

[FeFe]-hydrogenases catalyze the reversible conversion of protons and electrons to dihydrogen in biology.^[1,2] The crystal structures of the [FeFe]-hydrogenase from two bacteria, *Clostridium pasteurianum* (*CpI*)^[3–5] and *Desulfovibrio desulfuricans* str. *Hildenborough* (*DdH*),^[6–8] revealed that the catalytically active Fe-S cluster, named the H-cluster, is composed of a classical [4Fe-4S]-subcluster connected by means of a cysteine thiolate ligand to an organometallic [2Fe]-subcluster. The two iron centers in the [2Fe]-subcluster are coordinated by the terminal carbonyl and cyanide ligands and are linked together with a bridging carbonyl and a non-protein dithiolate ligand. The crystal structure of the [FeFe]-hydrogenase from *CpI* shows electron density at the apical coordination position of the distal iron of the [2Fe]-subcluster relative to the [4Fe-4S]-subcluster, which was refined as a water molecule. This distal water molecule was not identified in the [FeFe]-hydrogenase from *DdH*.

This can be rationalized by the different crystallization conditions used for *DdH* compared to *CpI* since the hydrogenase enzyme was in a more reduced state in *DdH* than in *CpI* and it is likely that the distal iron site in *DdH* is coordinated by a terminal hydride or even a dihydrogen ligand.^[8]

One of the last uncertain structural/compositional features of the H-cluster is the very nature of the dithiolate ligand. This question has already been discussed in detail^[5,9–11] due to its possible implications for the mechanism of the proton transfer or dihydrogen uptake/release, as well as the possible effect on the electronic structure of the catalytic cluster.^[12] Initially, this unique ligand of the [2Fe]-subcluster was described as sulfur atoms that are covalently connected by three light atoms with an experimental electron density that corresponds to approximately 10 electrons.^[3] In the characterization of the [FeFe]-hydrogenase from *DdH*, the ligand was first assigned as propanedithiolate (pdt).^[6] Later, this assignment was revised to dithiomethylamine (dtma).^[7] This was a chemically reasonable assignment since the amine group can act as a base for the proton-transfer into and from the distal iron site. This was supported by early computational studies that indicated the plausibility of the secondary amine group being involved in protonation of the distal iron site.^[13,14] Furthermore, a recent biomimetic study, which involved a symmetrical tetra-

[a] Department of Chemistry and Biochemistry, NASA Astrobiology Biogeochemistry Research Center, Montana State University, Bozeman, Montana 59717, USA

Supporting information for this article is available on the WWW under <http://dx.doi.org/10.1002/ejic.201100318>.

phosphane diiron model with dtma as the bridging ligand, established the thermodynamic preference of the terminal versus the bridging hydride to produce dihydrogen by means of the protonation of the secondary amine group.^[15]

Recently, the close to atomic resolution crystal structure of the [FeFe]-hydrogenase from *CpI* was evaluated by two independent computational studies.^[5,9] The first approach^[5] used the structure that best fitted the electron density and evaluated the geometric structures for numerous possible compositions of the bridgehead (X = CH₂, NH, NH₂⁺, O, and S as a control). It was found that the oxygen atom gave the most reasonable structural and energetic agreement with the close to atomic resolution crystal structure.

A more advanced computational refinement, which used the actual experimental electron density map,^[9] indicated that the best fit was the NH₂⁺ group with its spherical electron density. However, the former study indicated that by considering a realistic computational model of the entire H-cluster, which included its approximately 3.5 Å protein environment, there was a considerable energetic preference (10–14 kJ mol⁻¹) of an inverted bridgehead conformation relative to the crystallographically observed one. In this computational model the positively charged ammonium group points towards the [4Fe-4S]-cluster or the proximal Fe center of the [2Fe]-subcluster and forms a H-bonding interaction with the bridging cysteine residue (Cys503 in *CpI*). This was in contrast with the crystallographically determined conformation for both *CpI* and *DdH*, where the bridgehead group faces the distal Fe center and thus points away from the bridging cysteine thiolate or the [4Fe-4S]-cluster. Moreover, in the inverted conformation, the positively charged ammonium group would disrupt the bonding between the two subclusters, shut down the electron transfer from/to the [2Fe]-subcluster, and thus inhibit the catalytic reaction. Despite the differences between the benefits and the compromises of the above computational approaches, it is obvious that even the close to atomic resolution (1.39 Å) of the crystal structure of the [FeFe]-hydrogenases is not sufficient to distinguish between the subtle structural differences of the isoelectronic bridgehead groups. Therefore, the exact composition of the bridgehead group will most probably be unambiguously revealed by the elucidation of the biosynthetic molecular mechanism of the [2Fe]-subcluster.

Recent work by Silakov et al.^[10] provided an example of how electronic structural information that was derived from advanced EPR measurements can be used to probe the composition of the dithiolate ligand. Our earlier work also indicated that the chemical composition of the dithiolate ligand may play a role in fine tuning the electronic structure of the H-cluster.^[12] The ¹⁴N HYSCORE investigation of the oxidized state of the [FeFe]-hydrogenase from *DdH*, where the [2Fe]-subcluster is in the mixed-valence low-spin [Fe^IFe^{II}] oxidation state (S_t = 1/2), indicated the presence of three unique nitrogen environments with characteristic nuclear quadruple coupling constants (NQCC). These were assigned to the NH₃⁺ group of the Lys237 residue in close proximity to the distal cyanide ligand, to the nitrogen atom

of the distal cyanide ligand, and to the bridgehead group of the dithiolate ligand that was assumed to be dithiomethylamine (dtma). Furthermore, the synthesis of the mixed-valence biomimetic model complex [μ -(SCH₂)₂NCH₂CH₂-SCH₃](μ -CO)Fe₂(PMe₃)₂(CO)₃] by Erdem et al.^[16] allowed for the analysis of the paramagnetic signature of the secondary amine group without the interference of other nitrogen-containing ligands or residues from the protein environment. These measurements showed that the ¹⁴N NQCC and η parameters for a secondary amine bridgehead group in this [2Fe]-biomimetic model are close to those found for the oxidized metalloenzyme (H^{ox}).^[10]

In this work we carried out systematic investigations of the electron density topology and, in particular, the specific amount of atomic spin density localization at the bridgehead group for the free dithiolate ligand, a series of biomimetic [2Fe]-complexes with various ligand environments, and the entire H-cluster embedded in an approximately 3.5 Å protein environment using density functional theory (DFT) combined with advanced population analysis methods. The concept of atomic spin density is of great importance in coordination chemistry due to its role in the indication of spin states, effective oxidation states, and, thus, electron configuration as well as covalent nature of bonding. The ligand K-edge X-ray absorption spectroscopy (XAS)^[17] can provide direct quantitative values for the atomic spin densities through the determination of the covalency of the metal–ligand bonds if the transition dipole moment for a given core level excitation is known. While this technique can provide information about the ligand environment of a transition metal center regardless of its magnetic state, a serious limitation of N K-edge XAS is the overwhelming background from the N atoms of the protein matrix. As discussed above, advanced paramagnetic spectroscopic techniques, such as electron–nuclear double resonance (ENDOR) and electron spin echo envelope modulation (ESEEM), provide another way to get quantitative information about the atomic spin densities indirectly from the metal hyperfine and, preferably, the ligand super-hyperfine interactions.^[18] This technique is, however, limited to paramagnetic systems. Another direct way of determining the atomic spin densities is by analyzing the results of the electronic structure calculations from either the wave function-based methods (ab initio MO) or the density functional theory (DFT) calculations. Despite the convenience of using computational models and methods, the extrapolation of the theoretical atomic spin densities to experimental paramagnetic spectroscopic signatures is greatly affected by the nature of the population analysis methods, the selected levels of theory, the basis sets, the compositions of the density functionals, and so forth. In this paper we provide a comprehensive analysis of the effect of population analysis methods on the topology of the electron density for low-valent carbonyl and cyanide complexes relevant to the H-cluster structure and its spin polarization. A follow up study^[19] will evaluate the performance of various density functionals and basis sets at the sulfur K- and iron L-edges for a series of [2Fe]-complexes.

Methods

All of the calculations were performed starting from the crystal structure coordinates for $[\text{Fe}_2(\text{CO})_6(\mu\text{-SCH}_2\text{-NHCH}_2\text{S})]$,^[20] $[\text{Fe}_2(\text{CO})_6(\mu\text{-SCH}_2\text{OCH}_2\text{S})]$,^[21] $[\text{Fe}_2(\text{CO})_6(\mu\text{-SCH}_2\text{CH}_2\text{CH}_2\text{S})]$,^[22] $[\text{Fe}_2(\text{CO})_4(\text{CN})_2(\mu\text{-SCH}_2\text{NHCH}_2\text{S})]$,^[23] and $[\text{Fe}_2(\text{CO})_5\{(\mu\text{-SCH}_2)_2\text{NCH}_2\text{CH}_2\text{SMe}\}]$.^[24] The one-electron oxidized free ligands $[\text{SCH}_2\text{NHCH}_2\text{S}]^{1-}$ (dtma), $[\text{SCH}_2\text{OCH}_2\text{S}]^{1-}$ (dtme), and $[\text{SCH}_2\text{CH}_2\text{CH}_2\text{S}]^{1-}$ (pdt) were analyzed using (i) the coordinates of the crystal structure of the analogous [2Fe]-biomimetic model and (ii) the coordinates that were obtained after the optimization of the geometry. Throughout the text, relaxed structures correspond to molecules that have been obtained by the optimization of the geometry of the crystal structure in the gas phase, whereas fixed structures correspond to complexes where the atoms are fixed at their crystallographic positions (single point calculations). We used the puckering of the dithiolate ligand and the orientation of the bridgehead group to distinguish between the proximal and the distal iron sites. In order to be consistent with the crystallographically detected dithiolate ligand orientation, the iron site that is closer to the bridgehead group was considered to be distal and vice versa. It has been proposed that the H^{ox} state of the H-cluster contains a [2Fe]-subcluster with an unpaired electron^[25,26] and, thus, each diamagnetic $[\text{Fe}^{\text{I}}\text{Fe}^{\text{I}}]$ -model complex was also evaluated in its oxidized $[\text{Fe}^{\text{I}}\text{Fe}^{\text{II}}]$ -state.

For the paramagnetic, oxidized hexacarbonyl complexes an additional structure was considered, which was termed rotated throughout the text, where one of the apical carbonyl ligands was rotated into the bridging position and optimized similarly to the process of Bertini et al.^[27] Without discussing in detail, we found that at the BP86/TZVP level the one-electron oxidized mixed-valence $[\text{Fe}_2(\text{CO})_6(\text{pdt})]^{1+}$ and $[\text{Fe}_2(\text{CO})_6(\text{dtme})]^{1+}$ complexes show global minima for the rotated or inverted structure, while the one-electron oxidized $[\text{Fe}_2(\text{CO})_6(\text{dtma})]^{1+}$ complex shows an energetic preference (ca. 12 kJ mol⁻¹) for the non-rotated structure where both terminal CO ligands occupy apical positions.

Furthermore, the electronic structure calculations were carried out for the entire [6Fe]-cluster by using a more than 200-atom virtual chemical model of the protein embedded H-cluster.^[5] The atomic coordinates of each of the models with various dithiolate conformations are given in the Supporting Information. In addition to the four cysteine residues that connect the [6Fe]-cluster to the protein matrix, this model contained truncated models of the residues GLN195, GLY418, TRP303, LYS358, PRO324, GLN325, PRO301, HIS500, VAL504, THR356, and SER357 (in *CpI*). The structural optimizations were performed using the BP86 functional^[28–30] with the SDD basis set^[31] and the electron density was analyzed at the BP86/TZVP level. The positively charged $[\text{4Fe-4S}]^{2+}$ cubane was merged from two antiferromagnetically coupled rhombs using the Generalized Ionic Fragment Approach (GIFA) method.^[5,32] The GIFA method allowed for the convenient construction of the initial, localized broken symmetry electronic structure

and provided a reproducible method for the evaluation of various starting electronic structures. The Supporting Information provides the atomic coordinates of each of the fragments separately. The various magnetic coupling schemes for the two $M_s = \pm 9/2$ [2Fe-2S] rhombs and the $S = 1/2$ [2Fe]-subcluster converged to only three distinct solutions that could be illustrated by the top/bottom, front/back, and left/right coupling of the [4Fe-4S]-subcluster. For the sake of brevity, only the lowest energy broken symmetry state was used for the atomic spin density calculations for each of the dithiolate compositions. The iron sites labeled Fe1, Fe2, Fe3, and Fe4 correspond to those coordinated with the Cys300, Cys355, Cys499, and bridging Cys503 residues (in *CpI*), respectively.

The electron densities were calculated by using Gaussian09 Revision A.02^[33] with the BP86 functional^[28–30] and the TZVP basis set^[34] for all of the models, including the sizeable H-cluster model. This combination of functional and basis sets can reproduce the orbital composition data reasonably well from XAS measurements^[19] and advanced electron paramagnetic resonance properties^[35] of the biomimetic [2Fe]-model complexes. We anticipated that the use of a hybrid functional, such as the popular B3LYP, would not change the conclusions of this study as indicated by ref.^[10,35] The atomic spin densities within each molecule were interpreted by using Mulliken (MPA),^[36] Weinhold (NPA),^[37] and Bader's Atoms in Molecules (AIM)^[38] population analyses. The NPA valence orbital sets for the iron and sulfur atoms were 3d4s4p and 3s3p, respectively. The AIM results were obtained by using the program AIM-All^[39] with the ProAIM method.^[40–42] When necessary, the Promega^[41,42] method was used for integrating atoms that had trouble in connecting complex ring, bond, or cage critical points.

As a high-level correlated wave function-based ab initio method, complete active space (CAS) multi-reference calculations were performed by using the Natural Bonding Orbitals derived from the ROB86 reference wave function for the one-electron oxidized free ligand radical, $[\text{dtma}]^{1-}$. The active space was constructed by using the four bonding and four antibonding molecular orbitals of the S–C and C–N bonds and the four S-based and one N-based lone pairs (13 orbitals) that were occupied with 17 electrons. The similarly large CAS calculation for the biomimetic model complex with additional Fe d orbitals and electrons for $[\text{Fe}_2(\text{CO})_6(\text{dtma})]^{1+}$ is currently beyond our computational capabilities (26 orbitals and 31 electrons); however, the above calculation was already sufficient to validate the DFT calculations for the free ligands.

Results and Analysis

Our strategy for surveying the extent of the covalent interactions through the analysis of the spin density distributions was composed of initially investigating the electronic structure of the oxidized free ligand radicals. These calculations can provide an estimate for the upper limit of

the spin delocalization since the actual paramagnetic centers (S atoms) are only a methylene group away from the bridgehead group (X). In comparison, the extent of spin delocalization is expected to be reduced in a [2Fe]-complex relative to that of the free ligands, since the Fe centers are an additional atom away from the bridgehead group unless a direct interaction is present. Consequently, the free ligand calculations were extended with a systematic evaluation of the biomimetic [2Fe]-complexes and were compared to the most reasonable structure of the H-cluster within its protein environment. It is important to highlight that besides the conventional orbital-based MPA and NPA methods, the topology of the entire electron density was evaluated by using the Bader's Atoms-in-Molecule method, which separates the electron density into atomic basins according to the curvature of the electron density.

Free Ligands

In order to investigate the magnitude of the spin delocalization from the sulfur atoms to the bridgehead group as a function of composition and geometry, we carried out calculations for two of the conformations of the one-electron oxidized dithiolate ligands. The right-hand side of Figure 1 presents the structures with the ligands fixed in the crystallographic positions of the corresponding [2Fe]-complexes, while the left-hand side shows the structures of the fully optimized, unconstrained dithiolates. The major difference between these two sets was the shorter S...S and longer S...X distances in the fixed structures compared to the relaxed structures. The spin density was mainly localized at the sulfur atoms in the relaxed structures, whereas the atomic spin density on the bridgehead group is only a few percent as presented in Table 1. Therefore, the spin delocalization is limited in the one-electron oxidized free ligands. This was expected since the mixing of the sulfur 3p orbitals with the 2s/2p orbitals of the bridgehead group is limited. Considering that the spin delocalization takes place through the σ -bonds, the CH₂ bridgehead group will consequently show a larger spin density (2–5%) relative to the NH (1–2%) and the O (1% of an electron or 0.01 *e*) groups due to the lower effective nuclear charge of C versus N or O, which leads to an energetically preferred orbital overlap. The lack of significant (> 0.05 *e*) atomic spin density on the bridgehead group indicated the absence of any covalent or through-space spin polarization between the bridgehead group and the sulfur atoms despite the shorter S...X distance.

The constraint of the sulfur atoms into the positions of the corresponding biomimetic complexes (fixed geometry in Table 1) imposed strain on the dithiolate ligands that led to a slight increase (up to 0.02 *e*) in the spin delocalization towards the bridgehead group for X = NH and O, in contrast to that of X = CH₂. The anomalous behavior of the pdt ligand, where the spin density decreased upon constraint, could be rationalized by the elimination of any possibility for the S...C–C hyperconjugation that is present in

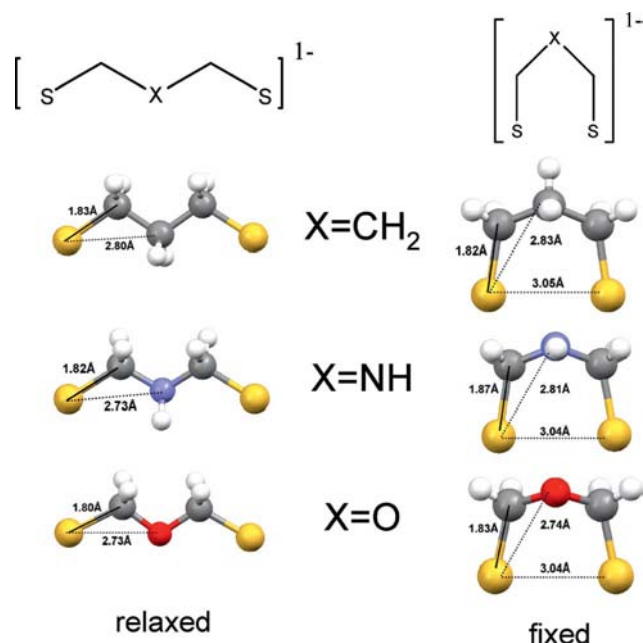


Figure 1. The structures of the free dithiolate ligands.

Table 1. A comparison between the atomic spin densities (% of an electron) for the free ligands with various bridgehead groups (CH₂, NH, O) as a function of the population analysis method and the optimization state (fixed: as in the corresponding [Fe^IFe^I]-clusters).

Population analysis	Optimization state	Bridgehead group (X)								
		CH ₂			NH			O		
		S	βCH ₂ X	S	βCH ₂ X	S	βCH ₂ X	S	βCH ₂ X	S
MPA	Fixed	99	–1	2	100	–1	1	100	–1	1
	Relaxed	98	–3	5	97	3	0	97	3	0
NPA	Fixed	98	0	2	100	0	1	100	0	0
	Relaxed	96	1	4	94	6	0	98	6	0
AIM	Fixed	96	2	2	97	2	2	97	2	1
	Relaxed	92	4	3	93	7	0	93	8	0

the flat relaxed structure (see the discussion below for the spin density distribution plots). Comparing the various population analysis methods, both the MPA and NPA methods can result in total negative spin densities due to the spin polarization that spans differently among the multiple spin up (α) and spin down (β) orbitals. Large deviations between these spin orbitals are generally indicative of either the multireference nature of the ground state wavefunction or a limitation of the given population analysis/basis set combination. However, by using the AIM method, the total spin density contributions from each of the atoms is positive and is significantly different (by 6% for S, for example) compared to when the popular MPA method was used. As discussed later, the AIM method does not completely eliminate the negative spin densities since it provides correct negative spin densities for the antiferromagnetically coupled iron centers in the [4Fe–4S]-subcluster.

Figure 2 summarizes the atomic spin density plots and the AIM topology maps of the total electron density. The relaxed structures of the one-electron oxidized free ligands

showed the anticipated bond critical points (green dots) along the bond pathways that connect the atoms according to the valence bond picture. The dashed versus solid line style for a bond pathway is indicative of the amount of electron density localized between two given atoms along a bond path and hence the weak versus strong nature of a bonding interaction, respectively. The appearance of small spin densities on the C–C and C–H bonds parallels the previously discussed orbital overlap considerations. The somewhat larger accumulation of spin density for the pdt ligand is due to the presence of the S...C–C hyperconjugation, while the same pathway does not exist for the heterometal-substituted dithiolates. Rather, the delocalization of the spin density takes place through the S...C–H path. The AIM results showed the emergence of a new bond critical point among the two sulfur atoms for the fixed geometry that corresponds to a weak sulfur-sulfur bonding interaction. Moreover, a ring-critical point (red dot) also emerged and is located approximately in the middle of each ring at about 3.24 Å away from the S atoms and the bridgehead group. Thus, from the topology features of the electron density and the spin density distributions, we concluded that the emergence of 0.02–0.03 *e* atomic spin density (Table 1) at the bridgehead group originates from the ring-strain effect of the dithiolate ligand, which creates a modest through-space delocalization pathway from the sulfur-centered radical into the bridgehead group.

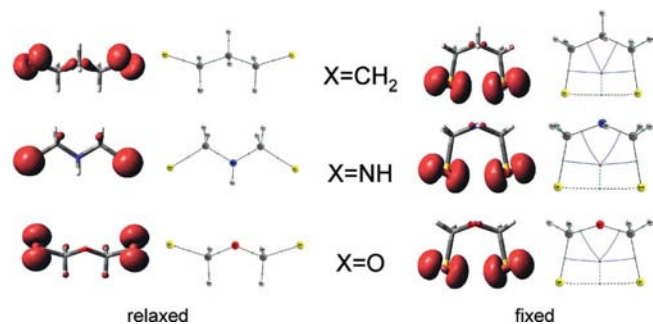


Figure 2. The atomic spin density plots and the AIM plots for the free ligand radical structures, $[\text{SCH}_2\text{XCH}_2\text{S}]^{1-}$.

In order to address the possible multireference nature of the dithiolate electronic structure and, thus, the configuration interactions of the σ -orbital framework, we carried out a complete active space SCF calculation for the $[\text{dtma}]^{1-}$ radical. Figure 3 illustrates the composition of the active space (13 orbitals and 17 electrons) and the final occupation numbers from the converged one-electron density matrix. From these CASSCF results it was apparent that there is only a small mixing (at most 0.07 *e*) of the occupied and unoccupied molecular orbitals in the relaxed structure. Similarly to the DFT calculations, we detected a slight increase (at most 0.08 *e*) in the fixed dithiolate geometry of the $[\text{2Fe}]$ -complexes. This indicated a limited delocalization of the spin density from the S lone pairs, through the S–C and C–N bonds, into the N lone pair. These conceptually higher-level calculations corroborated the DFT results and verified that the amount of spin density at the bridgehead

group of the one-electron oxidized free ligands is only a few percent. A similar agreement between the CASSCF and DFT calculations has been described for the entire $\text{Fe}_2(\text{CO})_6$ -(pdt) complex in the work of Bertini et al.^[27] using a smaller active space.


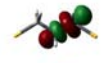
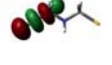
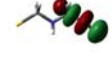
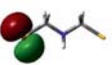
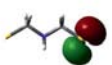



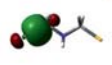
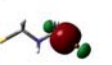
			RELAXED	FIXED
		— —	0.07 <i>e</i> [−]	0.08 <i>e</i> [−]
		— —	0.04 <i>e</i> [−]	0.04 <i>e</i> [−]
		⊕ ⊕	2.97 <i>e</i> [−]	3.01 <i>e</i> [−]
		⊕ ⊕	4.00 <i>e</i> [−]	3.98 <i>e</i> [−]
		⊕ ⊕	2.00 <i>e</i> [−]	1.97 <i>e</i> [−]
		⊕ ⊕	3.98 <i>e</i> [−]	3.96 <i>e</i> [−]

Figure 3. The ROBP86/NBO reference orbitals for the $[\text{SCH}_2\text{NHCH}_2\text{S}]^{1-}$ radical dithiolate that was used for the 13 orbitals and 17 electrons CASSCF calculations and the occupation of these orbitals from the one-electron density matrix.

Biomimetic $[\text{2Fe}]$ Complexes

In order to evaluate the presence of direct bonding interactions between the Fe centers and the bridgehead groups in the diamagnetic $[\text{Fe}^{\text{I}}\text{Fe}^{\text{I}}]$ -clusters, we carried out electron density topology analysis by AIM (Figure 4). This revealed additional ring critical points and related pathways, besides those expected by a valence bond picture. The presence of the Fe–Fe bond was apparent as indicated by a bond critical point approximately in the middle of the two iron centers. Besides the ring critical point already shown for the constrained one-electron oxidized dithiolate ligand in Figure 2, there are two more ring critical points that are located in the middle of each three-membered $[\text{Fe}–\text{S}–\text{Fe}]$ ring.

Importantly, despite the puckered nature of the metalladithiolate ring and the shorter distance between the bridgehead group and the distal Fe site versus the proximal Fe site, we did not find any direct bond path between the iron centers and the bridgehead group for the $[\text{Fe}^{\text{I}}\text{Fe}^{\text{I}}]$ oxidation state. However, we observed a slight skewing of the dithiolate ring critical point towards the distal iron center, regardless of the chemical composition of the bridgehead group. In order to investigate the potential importance of this non-planarity, we carried out a stepwise inversion of the bridgehead group for X = NH, as shown in the conformational energy diagram (Figure 5). As the dithiolate ring becomes flat, the corresponding ring critical point moves into the plane defined by the sulfur and carbon atoms, but with only a modest change in the atomic spin density at the bridgehead group from 0.19 to 0.15 *e*. The geometry that bears a

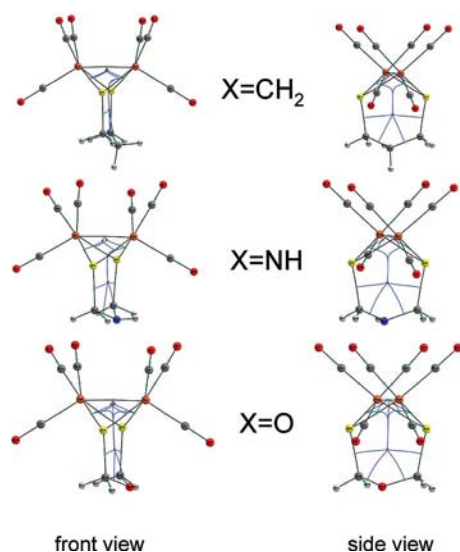


Figure 4. AIM electron density topology analysis of the $[\text{Fe}^{\text{I}}\text{Fe}^{\text{I}}]$ biomimetic complexes (the green and red dots are the bond and ring critical points, respectively).

coplanar $[\text{S}-\text{CH}_2-\text{NH}-\text{CH}_2-\text{S}]$ moiety (C_{2v} molecular symmetry, top right corner) corresponds to a second order transition state with respect to the amine N inversion ($573i\text{cm}^{-1}$) and the ring puckering inversion ($235i\text{cm}^{-1}$). Remarkably, this planar ring structure is ideal for the delocalization of the spin density from the paramagnetic iron centers through the sulfur lone pairs and C–H bonds into the out-of-plane N lone pair. For example, the incorporation of an allylic dithiolate group would enhance the covalent interaction between the bridgehead group and the Fe centers. The bottom right hand corner of Figure 5 shows the spin density distribution plot for the C_{2v} structure. The spin density lobes clearly indicate that the delocalization proceeds through the $\text{Fe}\cdots\text{S}\cdots\text{C}-\text{H}\cdots\text{N}$ LP conjugation pathway. Thus, this structure represents the maximum extent of the spin delocalization (about a third of the total spin density) from the paramagnetic iron centers into the bridgehead group within the given coordination environment. Therefore, the nonplanarity of the ring critical point can be one of the indications for the efficiency of the orbital overlap, which gives rise to the through-space spin polarization of the bridgehead group.

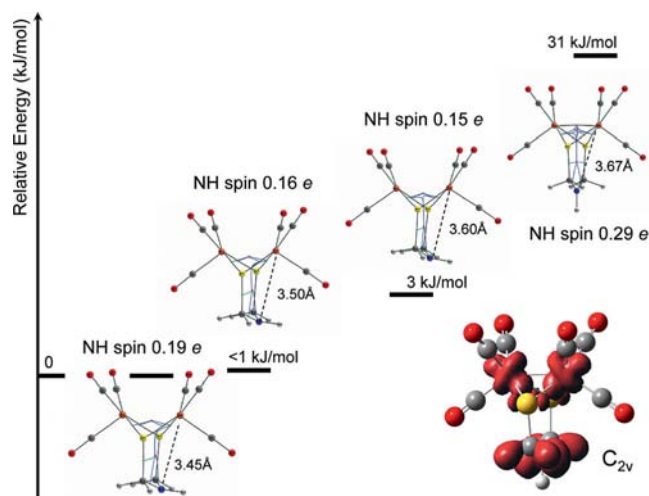


Figure 5. Potential energy surface for the inversion of the NH bridgehead group in the $[\text{Fe}^{\text{I}}\text{Fe}^{\text{II}}(\text{CO})_6(\text{dtma})]^+$ complex with the bridgehead group (NH) atomic spin densities and the AIM structures.

The relative energies for the inversion of the dithiolate ring puckering were in agreement with a small barrier for the inversion.^[43] This small barrier allows for the simultaneous presence of both bridgehead group orientations, which was manifested as a disorder in the crystal structure of the $[\text{Fe}_2(\text{CO})_6(\text{pdt})]$ cluster.^[22] In addition, a similar magnitude for the transition state energy was calculated for the $[\text{Fe}_2(\text{CO})_6(\text{pdt})]$ complex.^[27] This conformational change appears to be innocent for the biomimetic $[\text{2Fe}]$ complexes; however, as proposed earlier^[5] for a protonated bridgehead group (NH_2^+), this would result in a severe structural reorganization of the H-cluster.

In order to evaluate the spin density delocalization of the mixed valence $[\text{2Fe}]$ complexes in all three of the bridgehead compositions, the AIM analysis was carried out for the one-electron oxidized cationic $[\text{Fe}^{\text{II}}\text{Fe}^{\text{I}}]$ -clusters. Their optimized structures are shown in Figure 6 and the corresponding distances from the reduced $[\text{Fe}^{\text{I}}\text{Fe}^{\text{I}}]$ -clusters are shown in parentheses. A comparison between the AIM topology for the reduced and oxidized $[\text{2Fe}]$ complexes in Figure 4 and Figure 7, respectively, showed that upon one-electron oxidation the direct $\text{Fe}\cdots\text{Fe}$ bonding interaction vanishes, as indicated by the disappearance of the respective bond critical points and bond pathways between the two Fe centers.

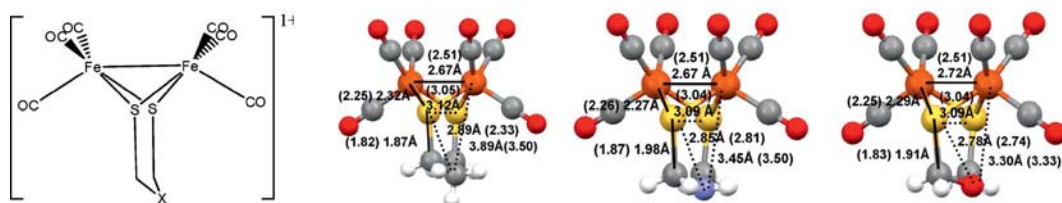


Figure 6. Optimized $[\text{Fe}^{\text{I}}\text{Fe}^{\text{II}}]$ biomimetic complex structures (the corresponding experimental distances for the $[\text{Fe}^{\text{I}}\text{Fe}^{\text{I}}]$ -complexes are shown in parentheses).

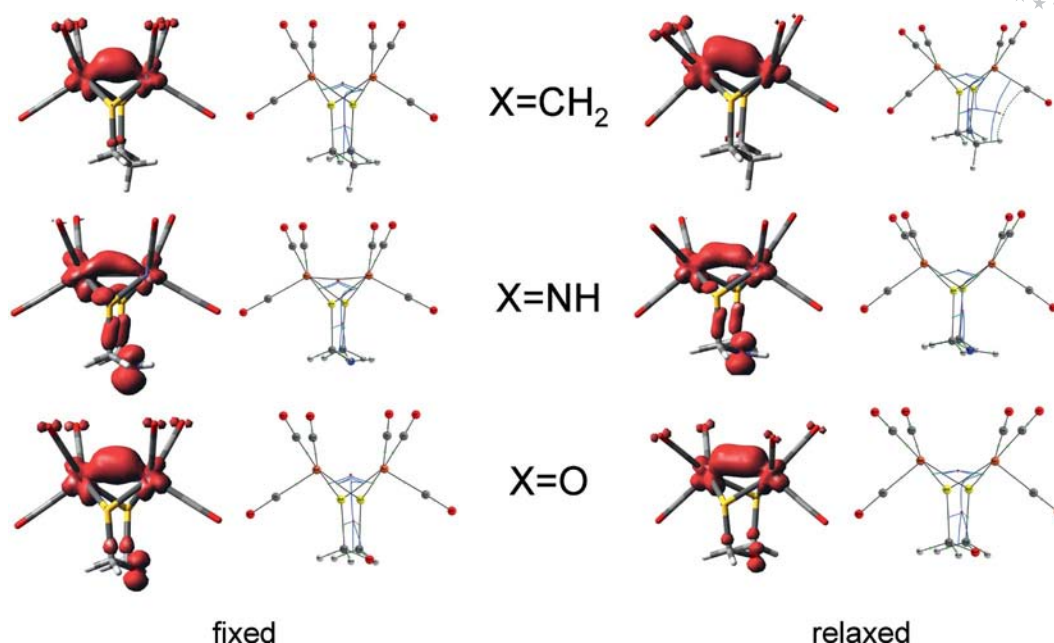


Figure 7. Summary of the atomic spin density contour plots and the AIM electron density topology of the $[\text{Fe}^{\text{I}}\text{Fe}^{\text{II}}]$ biomimetic complexes (the green and red dots are the bond and ring critical points, respectively).

Moreover, the $\text{Fe}\cdots\text{Fe}$ distances increased by 0.15 to 0.21 Å in the one-electron oxidized $[\text{Fe}^{\text{I}}\text{Fe}^{\text{II}}]$ complexes compared to those of the reduced $[\text{Fe}^{\text{I}}\text{Fe}^{\text{I}}]$ complexes, whereas the $\text{S}\cdots\text{S}$ distance only increased by 0.04 to 0.07 Å (Figure 6). These structural changes indicated that the $[\text{Fe}^{\text{I}}\text{Fe}^{\text{II}}]$ -cluster is electronically drastically different than expected upon a one-electron oxidation of the corresponding $[\text{Fe}^{\text{I}}\text{Fe}^{\text{I}}]$ -cluster, even without a large scale reorganization of the coordination environment. Since the $\text{Fe}\cdots\text{Fe}$ bond path is practically absent in the oxidized $[\text{2Fe}]$ complexes, the cluster is poised for structural rearrangement, such as the rotation of the $\text{Fe}(\text{CO})_3$ group, as has already been studied theoretically by Bertini et al.,^[27] or complete rearrangement, as experimentally shown by Heinekey et al.^[44]

Furthermore, the absence of the $\text{Fe}\cdots\text{Fe}$ bonding interaction for the relaxed $[\text{Fe}^{\text{I}}\text{Fe}^{\text{II}}]$ -cluster resulted in the collapse of the two $[\text{Fe}-\text{S}-\text{Fe}]$ ring critical points into a new one that sits in the center of the $[\text{Fe}-\text{S}-\text{Fe}-\text{S}]$ rhomb (Figure 7).

Importantly, the ring critical point of the dithiolate ligand remained the same, which suggests the presence of possible spin polarization on the bridgehead group. Upon examining the spin distribution plots for the $[\text{Fe}^{\text{I}}\text{Fe}^{\text{II}}]$ -clusters (Figure 7), we found that there is a significant spin density localization on the bridgehead group that decreases in going from NH (16–20%) > O (5–10%) > CH_2 (1–2% from Table 2). A similar trend has been described for the fixed free ligand radicals (see above); however, to a more modest extent.

The amplification of the spin polarization effect relative to the corresponding free ligands is a demonstrative example for the unique electronic structure of the $[\text{2Fe}]$ -subcluster of the H-cluster. The bridgehead group is linked to the redox active iron centers by means of through-space electron density delocalization, which is represented by the ring critical points in AIM. By comparing the optimized $[\text{Fe}^{\text{I}}\text{Fe}^{\text{II}}]$ -clusters (Figure 7, right hand column), the AIM

Table 2. A comparison between the atomic spin densities (% of an electron) for the one-electron oxidized biomimetic $[\text{2Fe}]$ -complexes, $[\text{Fe}^{\text{I}}\text{Fe}^{\text{II}}(\text{CO})_6(\text{SCH}_2\text{XCH}_2\text{S})]$, as a function of the population analysis method and the optimization state (fixed: as in the corresponding $[\text{Fe}^{\text{I}}\text{Fe}^{\text{I}}]$ -clusters).

Population analysis	Optimization state	Bridgehead group (X)											
		CH_2				NH				O			
		Fe	S	βCH_2	X	Fe	S	βCH_2	X	Fe	S	βCH_2	X
MPA	Fixed	85	−3	5	1	64	10	4	20	78	−1	5	9
	Relaxed	90	−7	4	1	66	6	5	18	85	−6	5	5
	Rotated	88	1	2	1	76	4	4	7	84	1	4	2
NPA	Fixed	76	−2	4	1	58	10	8	22	59	0	6	10
	Relaxed	84	−6	2	1	61	6	4	18	76	−6	8	6
	Rotated	84	2	0	0	71	6	2	7	80	2	6	3
AIM	Fixed	73	2	5	2	58	13	6	19	68	5	5	8
	Relaxed	80	−1	2	1	60	10	6	16	75	0	5	4
	Rotated	82	3	3	1	71	7	5	6	78	4	4	2

topology plots revealed an intriguing new interaction that served as a rationale for the lack of atomic spin density for the methylene bridgehead group. As the Fe \cdots Fe bond is broken by the one-electron oxidation, the terminal CO ligand forms a bond pathway with the methylene bridgehead group by means of a C–H \cdots CO-type of H-bonding interaction. This type of interaction is not unknown and has been proposed to be responsible for the crystal packing forces in organometallic carbonyl complexes.^[45,46] As discussed later, the involvement of the bridgehead group in an interaction that shows some covalent/orbital overlap character reduces the localization of the spin density on the bridgehead group.

We also evaluated the effect of rotating one of the carbonyl ligands into a bridging position. The rotational energy profile for the Fe(CO)₃ group is shown in Figure 8A and the corresponding AIM analysis and atomic spin density plots are shown in Figure 8B. It is important to note that the bridgehead group does not point in the same direction relative to the Fe site with the vacant apical position for all three of the dithiolates. As shown in Figure 8B for the lowest energy rotated conformers, the CH₂ bridgehead group in the pdt-containing complex points towards the rotated Fe site where spin density is mostly localized, while the other two complexes show the opposite orientation. Due to the lack of any indication in the AIM topology plots for the covalent agostic C–H \cdots Fe or N–H \cdots Fe H-bonding interactions, the orientation of the bridgehead group was rationalized by the presence of electrostatic lone pair-lone pair repulsion between the bridgehead group and the Fe^I site bearing the extra electron density. The presence of the γ -H in the pdt ligand is most probably responsible for a dipole/lone pair attraction. It is also remarkable that the spin density always accumulates on the Fe site with the vacant apical position, which can be formally considered to be the reduced Fe^I site. This can be rationalized by considering the d-orbital splitting in the square-pyramidal coordination environment. The low spin formally Fe^{II} site has a b₁²e⁴a₁⁰b₂⁰ electron configuration with doubly occupied d_{xy}, (d_{xz}, d_{yz}) orbitals and vacant d_{z²} and d_{x²–y²} orbitals.

This can maximize the CO σ -donation and backdonation from the occupied Fe d-orbitals to the CO π^* orbitals. This is important for stabilizing the Fe–CO bonding for a high valent Fe site. The reduced Fe^I site with a b₁²e⁴a₁¹b₂⁰ electron configuration actually weakens the Fe–CO σ -bond due to the partial occupation of the a₁ (d_{z²}) orbital, but the reduced positive charge allows for higher backdonation from the Fe to the CO π^* orbitals, which compensates for the loss of the bonding interaction and overall results in the increased stabilization of the complex. In addition, the bending of the rotated CO group may allow for some flexibility in forming the orbital overlap with the Fe d-orbitals and, thus, in accumulating the extra electron density.^[47]

Since the bridging CO ligand practically precludes the presence of an Fe–Fe bond, we see a considerable change in the electronic structure relative to the non-rotated forms. A major difference between the rotated and the non-rotated isomers is the existence of an asymmetrical Fe coordination environment with an apical vacant position. As can be seen in Table 2, in going from the fixed to the relaxed and then to the rotated structures, the spin density on the bridgehead atom is significantly reduced. Remarkably, this conformational effect is most exaggerated for the dtma ligand, where the bridgehead spin density drops from 0.19–0.22 *e* to 0.06–0.07 *e*. The considerably larger electronic structural change is also well represented by the topology map in Figure 8B, where the Fe \cdots Fe bond critical point is absent in the dtma complex in contrast to the pdt or the dtme analogues. The drastic change in the localization of the atomic spin density at the bridgehead group stems from the asymmetry between the two iron centers, hence the strong localization of the atomic spin density (ca. 0.70 *e*) at the rotated Fe site with a vacant apical coordination position, regardless of the bridgehead orientation and composition. While the effect of this conformational change on the electronic structure is remarkable, the amount of spin density (up to 0.07 *e*) calculated on the bridgehead is still considerable, which was also detected experimentally^[16,35] for biomimetic models. Another remarkable electronic structural feature of the rotated

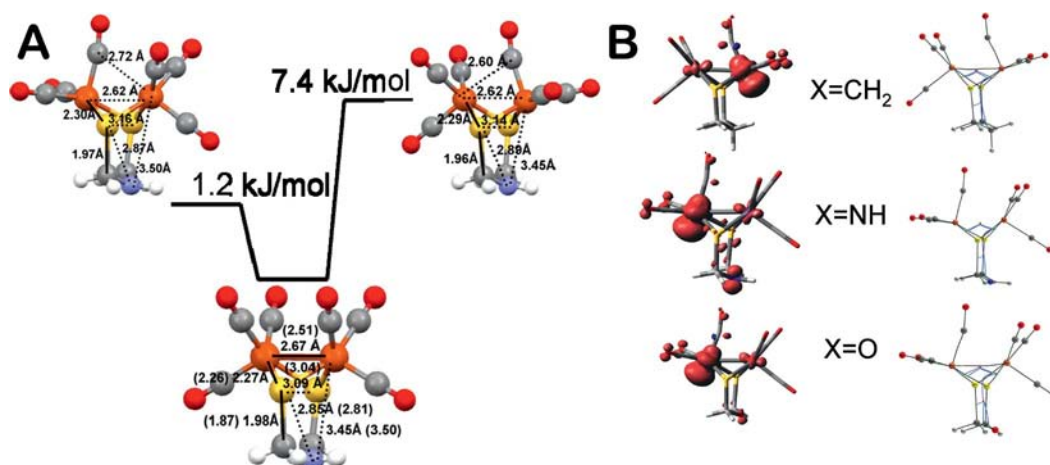


Figure 8. Conformational energy diagram for the Fe(CO)₃ group rotation (A) of the [Fe₂(dtma)(CO)₆] complex and (B) a comparison between the atomic spin density contour plots with the AIM electron density topology for the lowest energy rotated isomers.

conformer is the lack of a bond pathway between the formally bridging CO and the non-rotated Fe site, which indicated that the rotated CO can still only be considered as a terminal CO and not bridging in terms of covalent bonding.

The paramagnetic spectroscopic analyses of *DdH* indicated that the spin density is distributed over both of the iron centers in the H^{ox} state, but in the H^{ox} -CO state it is localized on the proximal iron site. In contrast, a more localized electronic configuration was found both experimentally and theoretically for the biomimetic models that have non-equivalent Fe sites.^[10,26,48] In order to account for the deviation between the spectroscopic properties of the biomimetic complexes and those of the protein bound active site, the presence of a distal ligand in the H^{ox} state of *DdH* should be considered since this would explain the spin density delocalization over the two Fe centers with a formal $Fe^{1.5+}$ oxidation state.^[49,50]

It is worth highlighting the differences between the various population analysis methods. Negative spin densities were observed for the complexes with CH_2 and O bridgehead groups. Since most of them disappeared when AIM was used, we attributed these spin densities to the limitation of a given population analysis method and basis set combination. The remaining negative spin density for the pdt-containing complex may be indicative of the presence of a non-negligible spin polarization. By comparing the Fe spin densities for the relaxed structures, we could generally say that the MPA results corresponded to the highest numbers and thus the most localized electronic structure, followed by the NPA results at approximately 7 to 10% reduced values. The AIM method further reduced the NPA results by approximately 2 to 5%. While we preferred the use of AIM for the analysis of the electronic structure of the transition metal complexes; the NPA method was also suitable especially since the former has not yet been adapted in many electronic structure packages.

Effect of Ligand Substitutions

In order to approach the actual ligand environment of the $[2Fe]$ -subcluster of the H-cluster, we examined the effect of the substitution of a carbonyl ligand with a cyanide or a thioether ligand. We chose these particular complexes, which bear dtma as the dithiolate bridge, due to the availability of their crystal structures.^[23,24] Figure 9 presents their optimized structures in the formally oxidized, paramagnetic $[Fe^I Fe^II]$ -oxidation states relative to their diamagnetic, crystallographically characterized states (the bond lengths are shown in parentheses). Table 3 summarizes the atomic/group spin density distributions as a function of the population analysis method and the composition for the one-electron oxidized states, and Figure 10 provides the overview of the atomic spin density distribution plots and the AIM electron density topologies. The considerable decrease in the spin density at the bridgehead group in the cyanide complex (0.06–0.09 e) versus its carbonyl analogue (0.16–0.22 e) was attributed to the network of intramolecu-

lar interactions formed by the bridgehead group and the apical cyanide groups. The formation of an $N-H\cdots\pi-CN$ interaction upon relaxation of the one-electron oxidized state manifested new bond pathways and, thus, an additional ring critical point appeared (left hand side of Figure 10). As this interaction connects the bridgehead group back to the paramagnetic center, the spin localization on the bridgehead group vanishes. Interestingly, we found that the spin density was delocalized into both of the cyanide ligands when they were fixed in their crystal structure positions and that this disappeared upon optimization of the geometry. This indicated that the reduced spin densities at the bridgehead group could not be due to the expansion of the singly occupied Fe-based orbital into the cyanide ligands since both the cyanide and the bridgehead ($X = NH$) spin densities decrease.

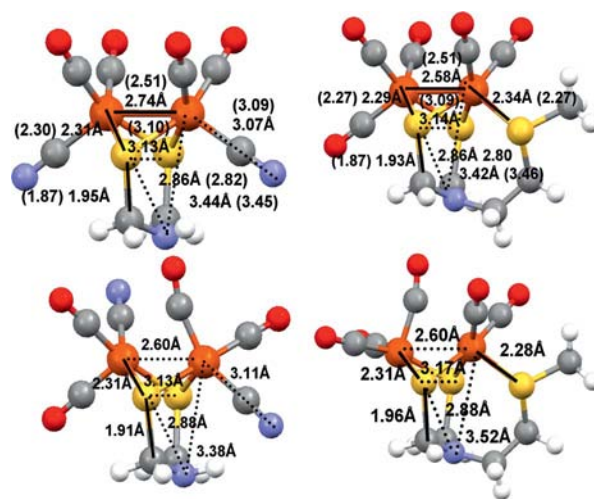


Figure 9. Optimized $[Fe^I Fe^II]$ biomimetic complex structures with a more realistic ligand environment with respect to the H-cluster (the corresponding experimental distances for the $[Fe^I Fe^I]$ -complexes are shown in parentheses).

The utility of using the ring critical points is well demonstrated by looking at the prototypical $[Fe_2S_3]$ -cluster with a slightly increased spin density at the bridgehead group (Table 3) relative to the corresponding hexacarbonyl $[2Fe]$ -complexes (Table 2) using the fixed $[Fe^I Fe^I]$ -geometry (Figure 10, top right hand corner). This calculation showed large spin density localization (0.22–0.25 e) on the bridgehead nitrogen and the appearance of two additional ring critical points related to the $[Fe-dithiolate-thioether-Fe]$ ring that are indicative of enhanced through-space delocalization pathways. Upon optimization (Figure 10, middle right hand structures), the latter two ring critical points merged into a single one and the bridgehead spin density dropped from a considerable value of 0.24 e to a low value of approximately 0.04 e , which is closer to those of the cyanide complex (ca. 0.09 e) than to those of the initial fixed structure of the hexacarbonyl $[2Fe]$ -complex.

It is also notable that the optimization of the $[Fe_2S_3]$ model complex alters its overall electronic structure. From the oppositely colored lobes of the Fe spin density in Figure 10 (middle right hand structures), it was clear that spin

Table 3. A comparison between the atomic spin densities (% of an electron) for the one-electron oxidized biomimetic [2Fe]-complexes with a more realistic ligand environment with respect to the H-cluster as a function of the population analysis method and the optimization state (fixed: as in the corresponding [Fe^IFe^I]-complexes).

Population	Optimization	[Fe ₂ (CO) ₄ L] ⁿ								
analysis	state	L = (CN) ₂ (μ ² -SCH ₂ NHCH ₂ S); <i>n</i> = −1					L = (CO) ₅ {(μ ² -SCH ₂) ₂ NC ₂ H ₄ SMe}, <i>n</i> = +1			
		Fe	S	N(CN)	^β CH ₂	NH	Fe	S	^β CH ₂	N
MPA	Fixed	86	−5	5	4	7	56	12	4	25
	Relaxed	79	−4	−1	5	9	95	1	6	4
	Rotated	92	7	9	2	0	80	4	4	6
NPA	Fixed	79	−4	8	8	6	45	13	6	25
	Relaxed	74	−4	1	4	8	89	3	3	4
	Rotated	86	8	10	2	1	74	6	4	7
AIM	Fixed	76	2	7	5	6	51	13	8	22
	Relaxed	69	2	1	6	8	89	6	6	3
	Rotated	85	8	8	1	0	74	7	4	5

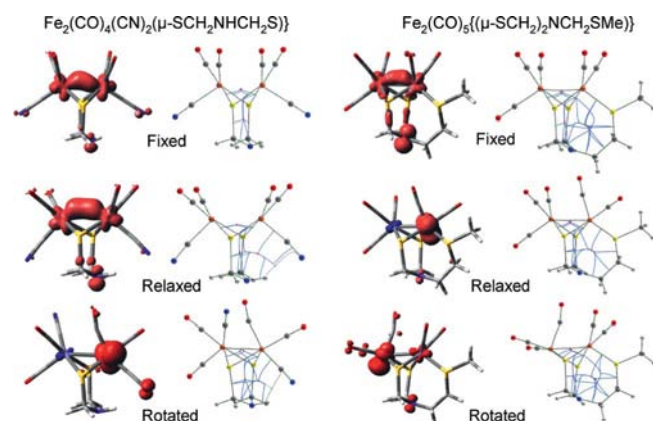


Figure 10. Summary of the atomic spin density contour plots and the AIM electron density topology of the [Fe^IFe^I] biomimetic complexes with a more realistic ligand environment with respect to the H-cluster (the green and red dots are the bond and ring critical points, respectively).

polarization occurs at the iron centers. The tricarbonyl coordinated iron site gained considerable negative spin density in addition to the rotation of the Fe 3d_{z²} orbital. This was also manifested in the relative position of the vicinal carbonyl ligands as the Fe(CO)₃ moieties rotated relative to each other around the Fe...Fe axis with an average OC–Fe...Fe–CO dihedral angle of 10 to 26°. However, the overall AIM topology of the electron density remains approximately the same with the exception of the coalescence of the ring critical points. Another remarkable feature of the thioether coordinated complex is that upon one-electron oxidation the Fe–Fe bond remains intact while in the carbonyl and cyanide complexes it is broken. This was rationalized by the considerable donation from the thioether to the Fe sites, which maintains enough electron density between the Fe centers for the existence of a covalent bond pathway.

Upon complete rotation of a carbonyl ligand into the bridging position (Figure 10, bottom structures), the atomic spin density at the bridgehead group disappears for the dicyanide substituted [2Fe]-complex, which is similar to the hexacarbonyl derivatives, due to the strong localization of the unpaired electron to the rotated Fe center and the adja-

cent apical cyanide ligand, as depicted in Figure 10 (bottom left hand corner). These electronic structural changes were explained by the AIM topology analysis as the cyanide nitrogen becomes the terminal point of a network of intramolecular interactions and thus accumulates atomic spin density. Remarkably, the spin density on the bridgehead group for the rotated [Fe₂S₃]-complex (Figure 10, bottom left hand structures) increased and the spin polarization disappeared compared to that of the relaxed non-rotated isomer (Table 3). It was also evident that there is spin localization at the rotated Fe center that is partially redistributed over the adjacent CO ligands; however, the topology of the electron density around the bridgehead group remains remarkably similar to that of the initial fixed structure (top right hand corner of Figure 10).

The electronic structure changes among the dicyanide-substituted and [Fe₂S₃]-clusters are important observations since these indicated that the presence of the intramolecular interaction networks, as represented by the bond pathways and ring critical points, is more effective in modulating the atomic spin density of the bridgehead group than the rotation of one Fe site. However, these clusters, which are structurally more analogous to the [2Fe]-subcluster, also exhibit localization of the spin density at the rotated Fe site (bottom of Figure 10), which is similar to the hexacarbonyl derivatives (Figure 8). The comparison between the atomic spin densities that were calculated for the rotated [Fe₂S₃]-complex with a vacant apical coordination position and the analogous, but coordinately saturated, [Fe₂S₃]-complex with the phosphane ligands^[16] (see Figure S1) revealed that the latter complex is electronically closer to the non-rotated hexacarbonyl [2Fe]-complexes with respect to the Fe 3d_{z²} orbital orientations as well as the atomic spin density distributions. These observations supported the assumption that the latter mixed-valence, phosphane-coordinated [Fe₂S₃]-complex^[16] is a close electronic structural mimic of the H-cluster in the H^{ox}-CO state.

H-Cluster

As a realistic model system of the H-cluster, we examined the atomic spin density distributions and the electron den-

sity topology of a more than 200 atom model of the [6Fe]-cluster with an approximately 3.5 Å protein environment that included various truncated amino acid residues and backbone amide groups. Figure 11 highlights the key differences in the distal Fe coordination environment as a function of the bridgehead group and the nature of the distal ligand. By starting from the published crystal structure (PDB code: 3C8Y),^[5] the optimization of the geometry could result in two different orientations of the distal water ligand. For the H-cluster structure with the pdt (Figure 11A) and dtma (Figure 11C) ligands, the hydrogen atoms of the bridgehead group form a H-bond with the water molecule, while one of the hydrogen atoms of the H₂O forms an agostic Fe···H–O bond. A reverse hydrogen-bonding interaction is present for the dtme-containing model (Figure 11F), where the H₂O is coordinated by means of the oxygen lone pair to the distal iron site as indicated by the shorter Fe···OH₂ distance (2.24 Å). Moreover, the oxygen bridgehead group is more than 0.1 Å closer to the distal iron site (Figure 10F) than for the other two compositions in Figure 11A and C. For the sake of probing the two extremes of the distal site coordination environment, we also examined the electronic structure of a computational model without the distal water molecule as crystallographically described for the H-cluster in *DdH* (Figure 11D and G) and with a carbonyl ligand as in the CO inhibited H^{ox}-CO state (Figure 11B and E).^[4]

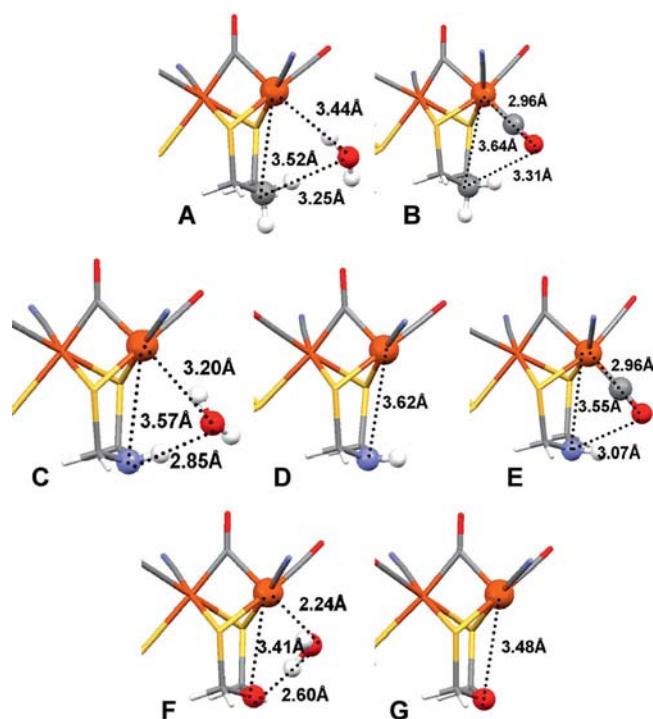


Figure 11. Comparison between the distal iron site of the H-cluster cut out from the 200+ atom virtual chemical model of the H-cluster and its immediate protein environment with respect to the distal ligand, distal iron, and bridgehead group distances.

Due to the presence of the conformational isomers with regards to the axial and equatorial N–H bond orientation relative to the metallacyclohexane ring that contains the

distal Fe site, both of the conformers were evaluated. We found that the H-cluster model where the distal water is H-bonded to the amine bridgehead group (Figure 11C) is energetically more favored by 7 kJ mol^{−1} compared to the conformer with an equatorial hydrogen atom. The CO-bound structure is practically energetically degenerate with regard to the orientation of the N–H bond. Finally, with regard to the isomers where the apical position is vacant, the structure where the hydrogen atom occupies an equatorial position is only 4 kJ mol^{−1} less stable than the structure shown in Figure 11D (axial N–H). For the sake of clarity and brevity, we have only reported the results for the lowest energy structures.

The AIM atomic spin density distributions that were calculated at the BP86/TZVP level for the BP86/SDD optimized, protein environment-embedded H-cluster model structures are shown in Table 4. Contrary to the observed trend for the biomimetic model complexes, we found a spin density of only about 0.002 *e* (0.2%) at the bridgehead group regardless of its composition. However, the atomic spin density of the distal iron gave a clear correlation with the coordination strength of the distal ligand. The strongly bound CO at the distal Fe site reduces the distal Fe spin density to about 0.28 *e* and increases the proximal Fe spin density to 0.42 *e*. This is a considerable change relative to the other models with the H₂O distal ligand. As we have discussed for the model complexes, the largest localization of spin density was found for the models without a distal ligand, which accumulates at a spin density of about 0.70–0.74 *e* at the distal Fe site and of about 0.19–0.21 *e* at the proximal Fe site. The CO-bound models have the most balanced distribution, which has already been found computationally by others;^[51] however, it contradicts the 5:1 distribution of spin between the proximal and distal Fe sites as interpreted from the spectroscopic data for the H^{ox}-CO state.^[26] The different distal water ligand coordination was also well represented by the changes in the atomic spin densities at the distal iron and the water ligand. The agostic Fe···H–OH interaction corresponds to an approximately 0.10 *e* increased Fe spin density in the pdt and dtma containing models, with a slight decrease of 0.02 *e* in the water spin density, relative to the normal Fe···OH₂ coordinative

Table 4. The atomic spin densities at selected centers of the H-cluster by AIM in the presence of the approximately 3.5 Å protein environment.

Distal	Bridgehead group (X)						
ligand	CH ₂		NH		O		
	H ₂ O	CO	H ₂ O	CO	None	H ₂ O	None
[4Fe-4S]	28.2	17.1	23.5	16.8	16.8	12.4	17.3
Fe ^{distal}	63.5	28.9	66.2	27.5	73.8	56.8	70.3
Fe ^{proximal}	14.2	42.3	15.0	43.3	21.4	33.0	19.0
2S	−0.2	13.5	0.1	14.2	−0.5	3.7	0.2
N (CN _{distal})	4.8	0.1	5.2	0.1	5.1	0.6	4.2
N (CN _{proximal})	0.0	0.0	0.0	0.0	−0.1	−0.1	−0.1
O(H ₂ O _{distal})	1.2	n/a	1.7	n/a	n/a	3.6	n/a
N (Lys358)	0.0	0.0	0.0	0.0	0.3	0.0	0.0
X	0.2	0.1	0.2	−0.1	0.2	0.1	0.2

bond in the dtme containing model. Interestingly, the bridging dithiolate sulfur spin density also varies as a function of the distal ligand and its interaction with the distal Fe site. A spin density of approximately $0.14 e$ is accumulated on the two sulfur centers in the $H^{ox}\text{-CO}$ models. This drops to about $0.04 e$ in the dtme containing model with the normal $Fe\cdots OH_2$ coordination and disappears if the distal water agostically binds to the distal Fe site or in the absence of a distal ligand.

It is important to note that variation in the coordination environment of the distal iron also affects the total atomic spin of the $[4Fe-4S]$ -subcluster. While formally this cluster is assumed to be diamagnetic in its $[4Fe-4S]^{2+}$ -state, non-negligible atomic spin density ($0.12\text{--}0.28 e$) can be delocalized from the $[2Fe]$ -subcluster by means of the bridging $S(\text{Cys})$ ligand as a function of the bridgehead group and the coordination environment of the distal site. In addition to this being a direct electronic structural support for the unique magnetic (spin)^[10] and electronic (orbital overlap)^[12] coupling between the $[4Fe-4S]$ and the $[2Fe]$ -subclusters of the H-cluster, the paramagnetic character of the $[4Fe-4S]$ -subcluster can spin polarize the neighboring H-bonded amino acid residues that have already been considered in the minimal environmental model of the H-cluster.

The remarkably complex AIM topology of the electron density in Figure 12 explained the lack of any spin density localization at the bridgehead group. The bridgehead group forms a strong, intermediate, and weak H-bonding interaction for the NH , O , and CH_2 composition with the distal water ligand as shown in Figure 11C, F, and A, respectively. The distal water loops the interaction network back to the paramagnetic distal iron site as represented by the appearance of a ring critical point that connects the entire distal site of the $[2Fe]$ -subcluster. The network of bond pathways transmits the spin polarization of the electron density and, thus, prevents the accumulation of spin density at the bridgehead group. Furthermore, the emergence of the ad-

ditional ring and even cage critical points (represented by blue dots in Figure 12) at the proximal side of the $[2Fe]$ -subcluster indicated a massive interaction network among the $[4Fe-4S]$ and $[2Fe]$ -subclusters that could not have been recognized previously from the molecular orbital-based analyses.^[12] These findings further substantiated that the H-cluster must be considered as an inseparable single molecule and not as two bridged $[Fe-S]$ -clusters. Furthermore, the modeling of the bridging thiolate link between the two clusters with thioether or a truncation of the H-cluster can only lead to results that have limited or no relevance to the actual catalytic active cluster of the $[FeFe]$ -hydrogenase.

Conclusions

The systematic evaluation of the electronic structures of the dithiolate ligand, biomimetic $[2Fe]$ -complexes in their one-electron oxidized forms, and the resting state ($S_t = 1/2$) of the entire $[6Fe]$ -framework of the H-cluster with a modest 3.5 \AA protein environment revealed remarkable features of the electron density topology and trends in the atomic spin density distributions from the three different population analysis methods. Among the Mulliken, Natural, and Atoms-in-Molecule population analysis methods, we found that the AIM method gave the most reasonable chemical interpretation of the electron and spin density features. Despite the valence bond considerations, we saw practically no atomic spin density accumulation on the bridgehead groups for the structurally relaxed, free dithiolate ligand radicals. However, the constraint of their geometry into a chelating position, as found in the corresponding $[2Fe]$ -complexes, resulted in the localization of the small, but non-negligible, atomic spin density on the CH_2 and NH groups. The limited spin polarization and the mixing of the occupied and virtual orbitals were confirmed with the multireference complete active space calculations, which reproduced the electronic structural differences in the fixed versus the relaxed DFT calculations.

With a slightly varied relative order, the trend that was found for the free ligands was continued for the biomimetic complexes despite the fact that the paramagnetic center was moved one atom farther away to the iron centers versus the sulfur centers in the free dithiolate ligands. Significant spin density was found for the secondary amine bridgehead group that was experimentally detectable by advanced paramagnetic techniques. The topology analysis of the molecular and spin electron densities by means of Bader's Atoms-in-Molecule method revealed the presence of the bond and ring critical points that graphically illustrated the through-space interaction between the paramagnetic iron centers and the bridgehead group by means of limited, but non-negligible, orbital overlap. The maximum extent of this interaction was well demonstrated by a hypothetical $[2Fe]$ -complex with a planar $[Fe-S-CH_2-NH-CH_2-S-Fe]$ dithiolate ligand as it formed a conjugated system of the Fe 3d orbitals, S 3p lone pairs, C-H orbitals, and N lone pair. Furthermore, we found that the spin delocalization dimin-

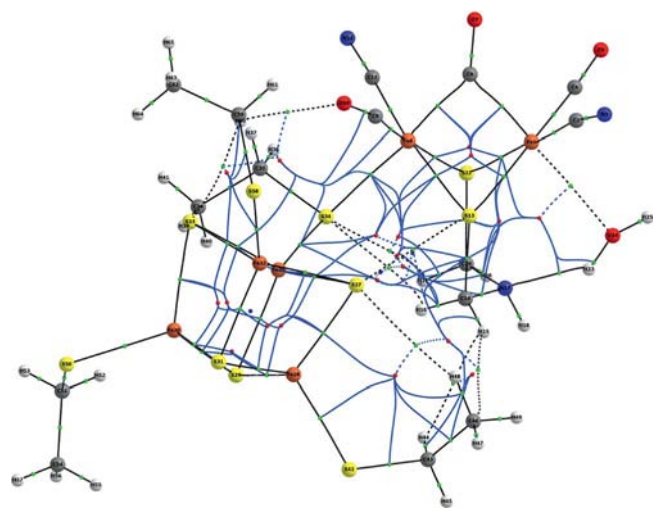


Figure 12. A "simplified" AIM electron density topology of the H-cluster with the additional interaction pathways between the protein environment and the cluster omitted for clarity.

ishes if the bridgehead group is involved in any intra- or intermolecular weak interactions, such as H-bonding. The rotation of an $\text{Fe}(\text{CO})_3$ site in the studied $[\text{2Fe}]$ -complexes further changed the electronic structure due to the strong localization of the spin density at the rotated Fe site with a vacant apical coordination position. This limited the through-space interaction between the paramagnetic iron site and the bridgehead group that lead to a considerable decrease in the atomic spin density. However, the atomic spin density and, most probably, the electronic coupling of the bridgehead group completely disappears if it becomes involved in a network of intramolecular covalent or H-bonding interactions. Remarkably, the virtual chemical model of the entire $[\text{6Fe}]$ -framework of the H-cluster showed an insignificant atomic spin density ($< 0.005 e$) at the bridgehead group regardless of the chemical composition of the dithiolate ligand or the distal ligand. However, the spin densities at the distal and proximal sites and their ratio are indicative of the nature of the distal ligand and its interaction with the distal Fe site. Similarly to the biomimetic complexes, a network of interactions that involved the bridgehead group would prevent the localization of the atomic spin density as the spin polarization is transmitted to a more terminal position if available or is looped back to the paramagnetic Fe centers. Importantly, the involvement of the bridgehead group in any network of H-bonds, dipole/charge, or any other weak interactions can have a great effect on the spin polarization within the cluster. Thus, the nature of the distal ligand, its interaction with the iron site as well as the bridgehead group, and the fine tuning effects of the neighboring amino acids to the H-cluster must be considered in any mechanistic investigation of the biological hydrogen uptake and evolution reactions by the $[\text{FeFe}]$ -hydrogenases.

Supporting Information (see footnote on the first page of this article): Atomic spin density plot of the mixed-valence, phosphane-coordinated $[\text{Fe}_2\text{S}_3]$ model complex synthesized by Erdem et al.^[16] and corresponding MPA atomic spin densities of the selected atoms, Cartesian coordinates of the 200+ atom model of the H-cluster and its about 3.5 Å protein environment broken down into individual molecular/ionic fragments, and Cartesian coordinates of all the one-electron oxidized structures in their relaxed geometries for the free dithiolate ligands and biomimetic $[\text{2Fe}]$ clusters.

Acknowledgments

This work was supported by a grant from the National Science Foundation CBET 0744820. The Astrobiology Biogeocatalysis Research Center is funded by NASA Astrobiology Institute Funded Grant NNA08C-N85A. We thank Dr. Todd Keith for the excellent support to AIMPro and the reviewers for their candid and constructive criticism of our manuscript.

- [1] P. M. Vignais, B. Billoud, J. Meyer, *Fems Microbiol. Rev.* **2001**, 25, 455–501.
- [2] M. W. W. Adams, *Biochim. Biophys. Acta* **1990**, 1020, 115–145.
- [3] J. W. Peters, W. N. Lanzilotta, B. J. Lemon, L. C. Seefeldt, *Science* **1998**, 282, 1853–1858.
- [4] B. J. Lemon, J. W. Peters, *Biochemistry* **1999**, 38, 12969–12973.
- [5] A. S. Pandey, T. V. Harris, L. J. Giles, J. W. Peters, R. K. Szilagy, *J. Am. Chem. Soc.* **2008**, 130, 4533–4540.
- [6] Y. Nicolet, C. Piras, P. Legrand, C. E. Hatchikian, J. C. Fontecilla-Camps, *Struct. Folding Des.* **1999**, 7, 13–23.
- [7] Y. Nicolet, A. L. de Lacey, X. Vernede, V. M. Fernandez, E. C. Hatchikian, J. C. Fontecilla-Camps, *J. Am. Chem. Soc.* **2001**, 123, 1596–1601.
- [8] Y. Nicolet, B. J. Lemon, J. C. Fontecilla-Camps, J. W. Peters, *Trends Biochem. Sci.* **2000**, 25, 138–143.
- [9] U. Ryde, C. Greco, L. De Gioia, *J. Am. Chem. Soc.* **2010**, 132, 4512–4513.
- [10] A. Silakov, B. Wenk, E. Reijerse, W. Lubitz, *Phys. Chem. Chem. Phys.* **2009**, 11, 6592–6599.
- [11] E. Pilet, Y. Nicolet, C. Mathevon, T. Douki, J. C. Fontecilla-Camps, M. Fontecave, *FEBS Lett.* **2009**, 583, 506–511.
- [12] D. E. Schwab, C. Tard, E. Brecht, J. W. Peters, C. J. Pickett, R. K. Szilagy, *Chem. Commun.* **2006**, 3696–3698.
- [13] H. J. Fan, M. B. Hall, *J. Am. Chem. Soc.* **2001**, 123, 3828–3829.
- [14] Z. P. Liu, P. Hu, *J. Am. Chem. Soc.* **2002**, 124, 5175–5182.
- [15] B. E. Barton, T. B. Rauchfuss, *Inorg. Chem.* **2008**, 47, 2261–2263.
- [16] Ö. F. Erdem, L. Schwartz, M. Stein, A. Silakov, S. Kaur-Ghumaan, P. Huang, S. Ott, E. J. Reijerse, W. Lubitz, *Angew. Chem. Int. Ed.* **2011**, 50, 1439–1443.
- [17] E. I. Solomon, B. Hedman, K. O. Hodgson, A. Dey, R. K. Szilagy, *Coord. Chem. Rev.* **2005**, 249, 97–129.
- [18] J. E. Huyett, S. B. Choudhury, D. M. Eichhorn, P. A. Bryngelson, M. J. Maroney, B. M. Hoffman, *Inorg. Chem.* **1998**, 37, 1361–1367.
- [19] L. J. Giles, A. Grigoropoulos, R. K. Szilagy, submitted to *J. Phys. Chem.*
- [20] J. L. Stanley, Z. M. Heiden, T. B. Rauchfuss, S. R. Wilson, L. De Gioia, G. Zampella, *Organometallics* **2008**, 27, 119–125.
- [21] L. C. Song, Z. Y. Yang, H. Z. Bian, Y. Liu, H. T. Wang, X. F. Liu, Q. M. Hu, *Organometallics* **2005**, 24, 6126–6135.
- [22] E. J. Lyon, I. P. Georgakaki, J. H. Reibenspies, M. Y. Darzensbourg, *Angew. Chem.* **1999**, 111, 3373; *Angew. Chem. Int. Ed.* **1999**, 38, 3178–3180.
- [23] H. X. Li, T. B. Rauchfuss, *J. Am. Chem. Soc.* **2002**, 124, 726–727.
- [24] J. D. Lawrence, H. X. Li, T. B. Rauchfuss, *Chem. Commun.* **2001**, 1482–1483.
- [25] W. Lubitz, E. Reijerse, M. van Gastel, *Chem. Rev.* **2007**, 107, 4331–4365.
- [26] A. Silakov, E. J. Reijerse, S. P. J. Albracht, E. C. Hatchikian, W. Lubitz, *J. Am. Chem. Soc.* **2007**, 129, 11447–11458.
- [27] L. Bertini, C. Greco, L. De Gioia, P. Fantucci, *J. Phys. Chem. A* **2009**, 113, 5657–5670.
- [28] A. D. Becke, *J. Chem. Phys.* **1993**, 98, 5648–5652.
- [29] J. P. Perdew, *Phys. Rev. B* **1986**, 33, 8822–8824.
- [30] Correction: J. P. Perdew, *Phys. Rev. B* **1986**, 34, 7406–7406.
- [31] M. Dolg, U. Wedig, H. Stoll, H. Preuss, *J. Chem. Phys.* **1987**, 86, 866–872.
- [32] R. K. Szilagy, M. A. Winslow, *J. Comput. Chem.* **2006**, 27, 1385–1397.
- [33] M. J. T. Frisch, G. W. H. B. Schlegel, G. E. Scuseria, M. A. Robb, J. R. Cheeseman, G. Scalmani, V. Barone, B. Mennucci, G. A. Petersson, H. Nakatsuji, M. Caricato, X. Li, H. P. Hratchian, A. F. Izmaylov, J. Bloino, G. Zheng, J. L. Sonnenberg, M. Hada, M. Ehara, K. Toyota, R. Fukuda, J. Hasegawa, M. Ishida, T. Nakajima, Y. Honda, O. Kitao, H. Nakai, T. Vreven, Montgomery Jr., J. A. J. E. Peralta, F. Ogliaro, M. Bearpark, J. J. Heyd, E. Brothers, K. N. Kudin, V. N. Staroverov, R. Kobayashi, J. Normand, K. Raghavachari, A. Rendell, J. C. Burant, S. S. Iyengar, J. Tomasi, M. Cossi, N. Rega, N. J. Millam, M. Klene, J. E. Knox, J. B. Cross, V. Bakken, C. Adamo, J. Jaramillo, R. Gomperts, R. E. Stratmann, O. Yazyev, A. J. Austin, R. Cammi, C. Pomelli, J. W. Ochterski, R. L. Martin, K. Morokuma, V. G. Zakrzewski, G. A. Voth, P. Salvador, J. J. Dannenberg, S. Dapprich, A. D. Daniels, Ö. Farkas, J. B.

- Foresman, J. V. Ortiz, J. Cioslowski, D. J. Fox, *Gaussian 09, Revision A.2*, Gaussian, Inc., Wallingford CT, **2009**.
- [34] A. Schafer, C. Huber, R. Ahlrichs, *J. Chem. Phys.* **1994**, *100*, 5829–5835.
- [35] A. Silakov, J. L. Shaw, E. J. Reijerse, W. Lubitz, *J. Am. Chem. Soc.* **2010**, *132*, 17578–17587.
- [36] R. S. Mulliken, *J. Chem. Phys.* **1955**, *23*, 1833–1840.
- [37] J. P. Foster, F. Weinhold, *J. Am. Chem. Soc.* **1980**, *102*, 7211–7218.
- [38] R. F. W. Bader, *Atoms in Molecules – A Quantum Theory*, Oxford University Press, Oxford, **1990**.
- [39] T. A. Keith, *AIMAll (Version 10.06.21)*, **2010**, <http://aim.tkgristmill.com>.
- [40] F. W. Biegler-König, R. F. W. Bader, T. H. Tang, *J. Comput. Chem.* **1982**, *3*, 317–328.
- [41] T. A. Keith, “Computational Improvements for the Theory of Atoms in Molecules” in the Ph. D. Thesis: *Molecules in Magnetic Fields* **1993**, pp. 176–213.
- [42] T. A. Keith, “Advances in QTAIM Calculations Using AIM-All”, <http://aim.tkgristmill.com/references.html>, to be published.
- [43] The organometallic active site of [Fe]hydrogenase: Models and entatic states. M. Y. Darensbourg, E. J. Lyon, X. Zhao, I. P. Georgakaki, *Proceedings of the National Academy of Sciences of the United States of America* **2003**, *100*, 3683–3688.
- [44] I. Aguirre de Carcer, A. DiPasquale, A. L. Rheingold, D. M. Heinekey, *Inorg. Chem.* **2006**, *45*, 8000–8002.
- [45] G. S. McGrady, G. Guilera, *Chem. Soc. Rev.* **2003**, *32*, 383–392.
- [46] J. C. M. Rivas, L. Brammer, *Coord. Chem. Rev.* **1999**, *183*, 43–80.
- [47] C. Makedonas, C. A. Mitsopoulou, *Eur. J. Inorg. Chem.* **2007**, 110–119.
- [48] W. Lubitz, W. Tumas, *Chem. Rev.* **2007**, *107*, 3900–3903.
- [49] A. K. Justice, M. J. Nilges, T. B. Rauchfuss, S. R. Wilson, L. De Gioia, G. Zampella, *J. Am. Chem. Soc.* **2008**, *130*, 5293–5301.
- [50] C. M. Thomas, T. B. Liu, M. B. Hall, M. Y. Darensbourg, *Inorg. Chem.* **2008**, *47*, 7009–7024.
- [51] A. T. Fiedler, T. C. Brunold, *Inorg. Chem.* **2005**, *44*, 9322–9334.

Received: December 20, 2010

Published Online: May 13, 2011